Geophys. J. Int. (2004) **158,** 1041–1052 doi: 10.1111/j.1365-246X.2004.02351.x

Spatio-temporal evolution of induced seismicity at Açu reservoir, NE Brazil

A. F. do Nascimento,[1,*] P. A. Cowie,[1] R. J. Lunn[2] and R. G. Pearce[1]

[1] *The University of Edinburgh, Department of Geology and Geophysics, West Mains Road, Edinburgh,* EH9 3JW, *UK*
[2] *Heriot-Watt University, Department Department of Civil and Offshore Engineering, Riccarton, Edinburgh,* EH14 4AS, *UK*

Accepted 2004 April 25. Received 2004 March 25; in original form 2003 February 24

SUMMARY

We present the spatio-temporal evolution of seismicity recorded by eight three-component digital seismographs in operation continuously during a 3 yr period (1994 August to 1997 May) at Açu reservoir, NE Brazil. The Açu dam is a 34 m high earth-filled dam constructed in 1983 May on an area of Precambrian shield. Based on seismic monitoring between 1987 and 1989 using single-component analogue seismographs, previous workers concluded that the seismic activity was a case of reservoir-induced seismicity (RIS) associated with diffusion of pore fluid pressure beneath the reservoir. The digital data presented here reveal the seismic activity in remarkable detail with vertical and horizontal location errors $\approx$0.1 km. A total of 286 events were recorded by three or more stations and all occurred at a depth of $<$5 km. Using these data we demonstrate that the majority of the earthquake activity is clustered within several well-defined zones and that individual zones are active over discrete periods of time. Over the entire period of seismic monitoring between 1987 and 1997 there is no simple correlation between reservoir level and number of seismic events. Lateral migration of the locus of seismic activity in an unpredictable fashion is shown to be partly responsible for the poor correlation, as event detection is not uniform through time. We also show that the time delay between maximum water level and a subsequent increase in seismic activity varies systematically; longer time delays correspond to activation of an earthquake cluster with a greater average hypocentral depth. However, within any one cluster there is no correlation between time delay and depth. The 3-D distribution of seismic activity through time may only be explained in terms of triggering by the diffusion of pore fluid pressure if the rock properties (e.g. permeability, strength) are heterogeneous.

Key words: diffusion, permeability, reservoir-induced seismicity, triggered seismicity.

1 INTRODUCTION

Dam-induced seismicity has received special attention from engineers and geoscientists because of its potential to damage constructions and nearby buildings, leading to human and material losses. Following damaging reservoir-induced seismicity (RIS) in the 1960s at Koyna (India), Hsingfengkiang (China), Kariba (Zimbabwe) and Kremasta (Greece), (see Gupta 1992, for review), a great improvement in seismic monitoring occurred and in the 1970s local seismographic station networks were deployed to monitor several reservoirs (Gough 1969; Gough & Gough 1970; Beck 1976; Talwani 1976). These led to lower detection thresholds and improved hypocentral locations of seismic events. Complementary field studies identified the factors that are likely to control the observed RIS: ambient stress field conditions, fracture occurrence, hydromechanical properties of the rocks beneath the reservoir, geology of the area, dimensions of the reservoir and lake-level fluctuations (Zoback & Hickman 1982; Talwani 1997). Observational and theoretical models, e.g. Bell & Nur (1978); Roeloffs (1988); Talwani (1997) attest to the existence of two effects when a water reservoir is filled: (i) the change in ambient stress condition as a result of the load of the water, which may lead to failure; (ii) the increase of interstitial pore pressure in the rock matrix, fractures and faults beneath the reservoir. This second effect arises from fluid diffusion, compaction of the water saturated rock as a result of the weight of the reservoir, or both. Therefore, the analysis of RIS potentially provides an excellent opportunity to investigate mechanical and/or hydraulic properties of the crust, e.g. Bell & Nur (1978), Talwani & Acree (1984), Roeloffs (1988), Talwani (1997), Chen & Talwani (2001).

*Now at: Universidade Federal do Rio Grande do Norte, Programa de Pós-Graduação em Geodinâmica e Geofísica, Campus Universitário Lagoa Nova, Natal, RN, 59078-970, Caixa Postal 1596, Brazil. E-mail: aderson@dfte.ufrn.br

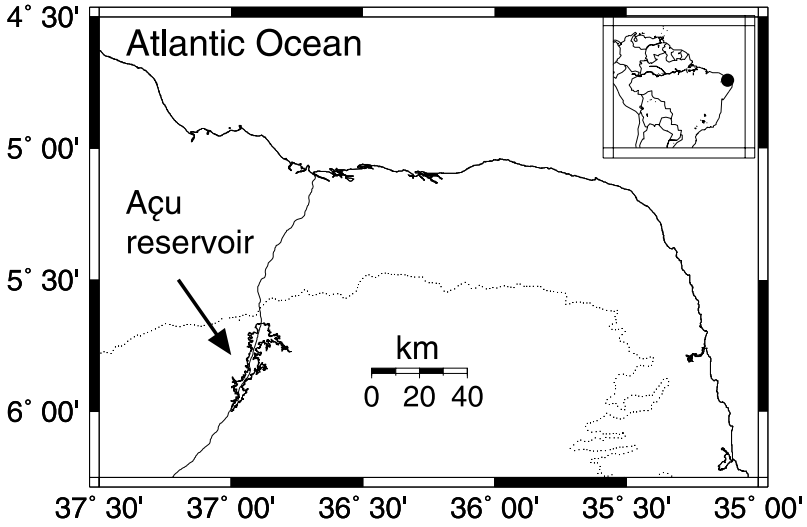

Figure 1. Map showing the location of the Açu reservoir in northeastern Brazil. The dotted line is the limit of the sedimentary basins that form the continental margin, e.g. Potiguar basin north of Açu.

Observational investigations of RIS are often jeopardized by the lack of accurate hypocentral locations. This is caused either by the complexity of the velocity structure in the area investigated or by the lack of appropriate seismic surveillance: i.e. the number, or the arrangement of seismic stations. Accurate hypocentral location and continuous seismic monitoring are important because they give information on significant aspects of RIS, such as migration of seismicity with time. In many cases of RIS, such as those reported by Gupta (1992) for example, only the number of events recorded by a single station is available. Hence, it could be that a clear correlation of water level with increased seismicity is masked out by the lack of control on the epicentral location of seismic events. In this respect the seismic monitoring described in this paper from Açu reservoir in NE Brazil (Fig. 1) has resulted in a very well-documented case of RIS. The combination of (i) continuous monitoring with a network of three-component digital seismographs over several years (1994–1997) and (ii) the simple velocity structure of the Precambrian basement in the Açu area reveals a detailed picture of the spatio-temporal evolution of seismic activity over several annual cycles of water level fluctuation.

Ferreira *et al.* (1995) first documented seismic activity associated with the construction of the Açu reservoir. It is located in an area of the Precambrian shield composed of paragneiss, biotite gneiss, gneiss-migmatite of Archean age and biotite granite of Neoproterozoic age (Jardim de Sá 1994). The area surrounding the dam has very flat topography. Hence the dam itself is fairly small (34 m) and the reservoir volume is only 2.4×10^9 m^3. The dam was completed in 1983 but the water level reached the spillway for the first time in 1985 February. It is not known exactly when the local seismic activity began but seismic monitoring began in 1987 August. From 1987 to 1989 only the number of seismic events was recorded using a single station. Over the next 8 yr two field campaigns, using single-component smoked-drum recorders, were carried out during 1989 October to December and 1990 November to 1991 March (Ferreira *et al.* 1995). These authors showed that the seismic activity occurred preferentially with dextral strike-slip focal mechanisms on NE oriented faults under regional E–W compression. Based on a preliminary result that indicated a correlation between reservoir level and seismicity (Fig. 2), Ferreira *et al.* (1995) concluded that the seismicity was a case of RIS. During the intervening periods only the total number of events was again recorded by a single permanent station BA1 (location shown in Fig. 3).

Ferreira *et al.* (1995) show a map of structural lineations, trending approximately NE in this area. They were derived from previous maps (CPRM 1980; Petrobras 1986) and satellite images. These lineations correspond to Precambrian ductile shear zones. More recently, Amaral (1997) presented field evidence that some of these ductile shear zones may have been reactivated as brittle faults at shallow crustal levels. The fabrics in the fault breccia indicate formation between 0 and 4 km in depth. According to Amaral (1997), the possible age of the brittle faulting is Cretaceous, although it is hard to constrain.

Fig. 2 shows the monthly variation of water depth and seismic activity, as recorded by BA1 for the entire period of seismic monitoring from 1987 to 1997. The horizontal two-headed arrows near the time axis indicate the duration of the field campaigns carried out by Ferreira *et al.* (1995) and by the present research (1994–1997). From 1987 to 1989, both the reservoir water level and the seismic activity showed a fairly simple quasi-periodic behaviour. According to Ferreira *et al.* (1995), the seismicity had a maximum correlation coefficient of 0.55 with the water level, with a delay of 3 months over this time interval. The value 0.55 is lower than might be expected from visual examination of Fig. 2 over the period 1987–1989, but this is largely a result of the different shapes of the two curves being correlated. The correlation of seismic activity with water level for the period 1987–1989 led Ferreira *et al.* (1995) to conclude that the diffusion of pore fluid pressure is the dominant mechanism for earthquake triggering in this area. However, from 1990 until 1997, the seismicity no longer shows such a clear correlation with the water level (Fig. 2). While periods of drought in 1990 and 1993 can explain some of the poor correlation, this explanation does not apply to other years, such as 1995 and 1996 when no drought occurred. Ferreira *et al.* (1995) suggested that another factor affecting the correlation was the migration of the locus of seismic activity so that event detection, using a fixed network geometry, would not be uniform through time. These authors demonstrated that a key characteristic of the Açu seismicity is the migration between discrete fault zones (Fig. 3), although their interpretation of this phenomenon was limited by relatively large location errors (≈0.5 km horizontal, but very poor vertical control).

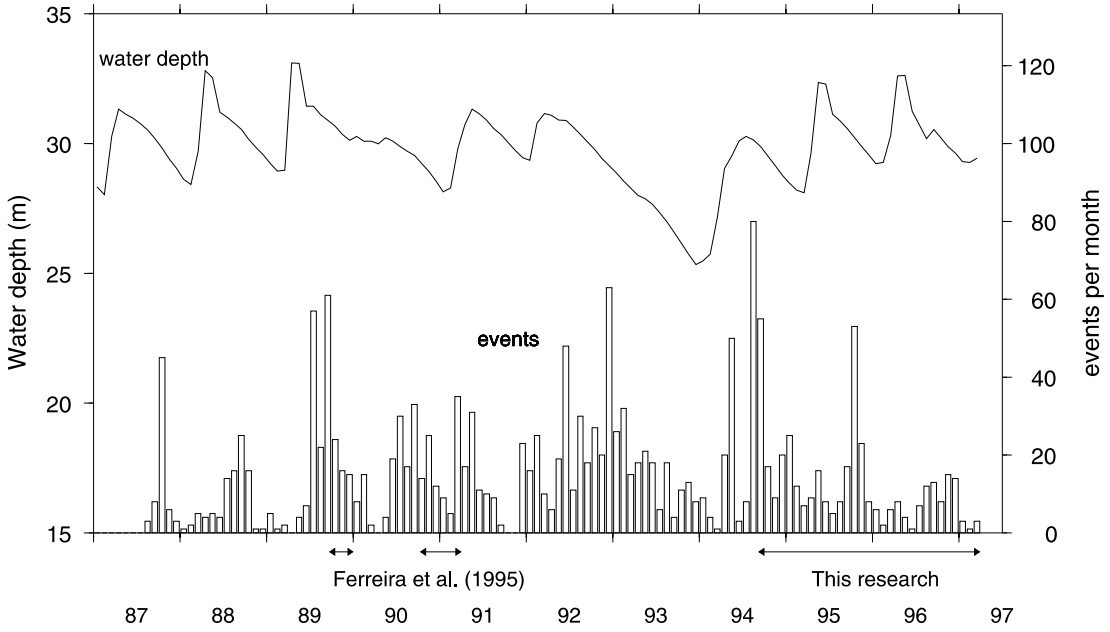

Figure 2. Monthly variation of reservoir water depth (top line) and monthly seismic activity (histograms) as recorded by station BA1 (shown in Fig. 3). The horizontal two-headed arrows near the time axis indicate the duration of the field campaigns carried out by Ferreira *et al.* (1995) and the present research. Water level data are from DNOCS–Depto. Nacional de Obras Contra a Seca, Brazil.

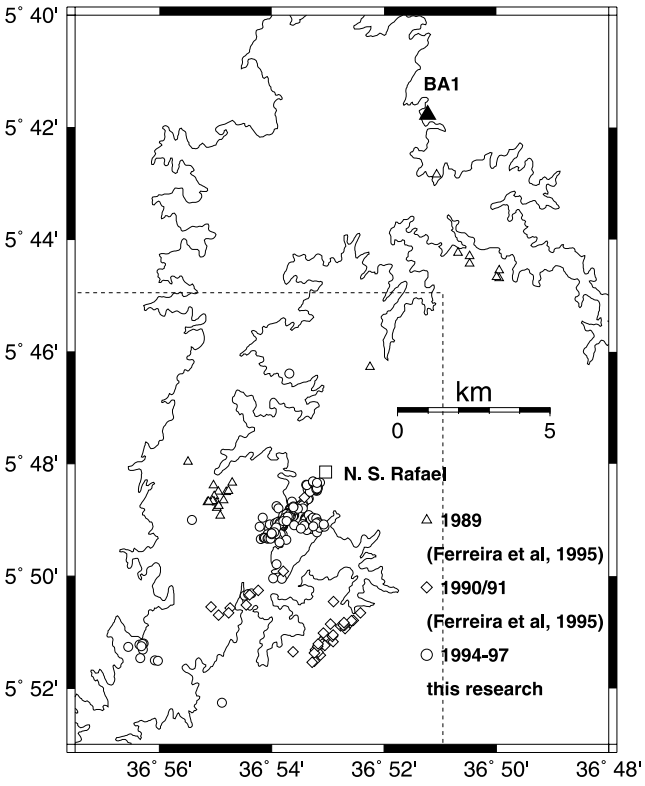

Figure 3. Pattern of seismicity in the Açu area recorded during three field campaigns. Triangles represent the 1989 epicentres, diamonds are the 1990/91 events documented by (Ferreira *et al.* 1995). Circles are the epicentres determined using the digital seismic network from 1994 until 1997 that are analysed in this paper. The permanent station BA1 is shown by the black triangle. The dashed line delimits the area where the digital network was installed.

In contrast, the location errors obtained with the three-component digital network are on average ≈0.1 km, for both vertical and horizontal, as we show below. Because of the improved location control we are now able to investigate both lateral and vertical migration of seismicity in great detail and show how the migration pattern relates to the reservoir water level as it fluctuates through time.

2 EVENT LOCATION AND FOCAL MECHANISM

Fig. 3 shows a summary of the seismic activity over the entire time interval of seismic monitoring in the Açu area (1987–1997). The locations of all the events were determined using the programme HYPO71 of Lee & Lahr (1975). Note that in map view (Fig. 3) the seismic activity is clustered in discrete NE trending zones and that different clusters are active over different time periods. Based on the data prior to 1991, Ferreira *et al.* (1995) suggested that there was a systematic migration of activity to greater distances from the reservoir. However, Fig. 3 shows that this is not in fact the case, an observation that we discuss further below.

Five different configurations of the digital network were used between 1994 November and 1997 April (Fig. 4). The dashed lines on each map of Fig. 4 denotes the approximate extent of the digital network, i.e. the approximate detection limit of the digital network. In other words, no events were located by the digital seismic network beyond the area defined by the dashed lines. The minimum, mean and maximum magnitude of the events detected by the network are, respectively: 0.13, 0.88 and 2.14. The time period during which each configuration of the digital network was deployed is also shown in Fig. 4. The reason for changing the network configuration is to reduce the station spacing and thus minimize the possibility of having an upper depth limit on the event location caused by a combination of velocity model choice and limitations on location theory. To effectively locate the depth of an earthquake, at least one

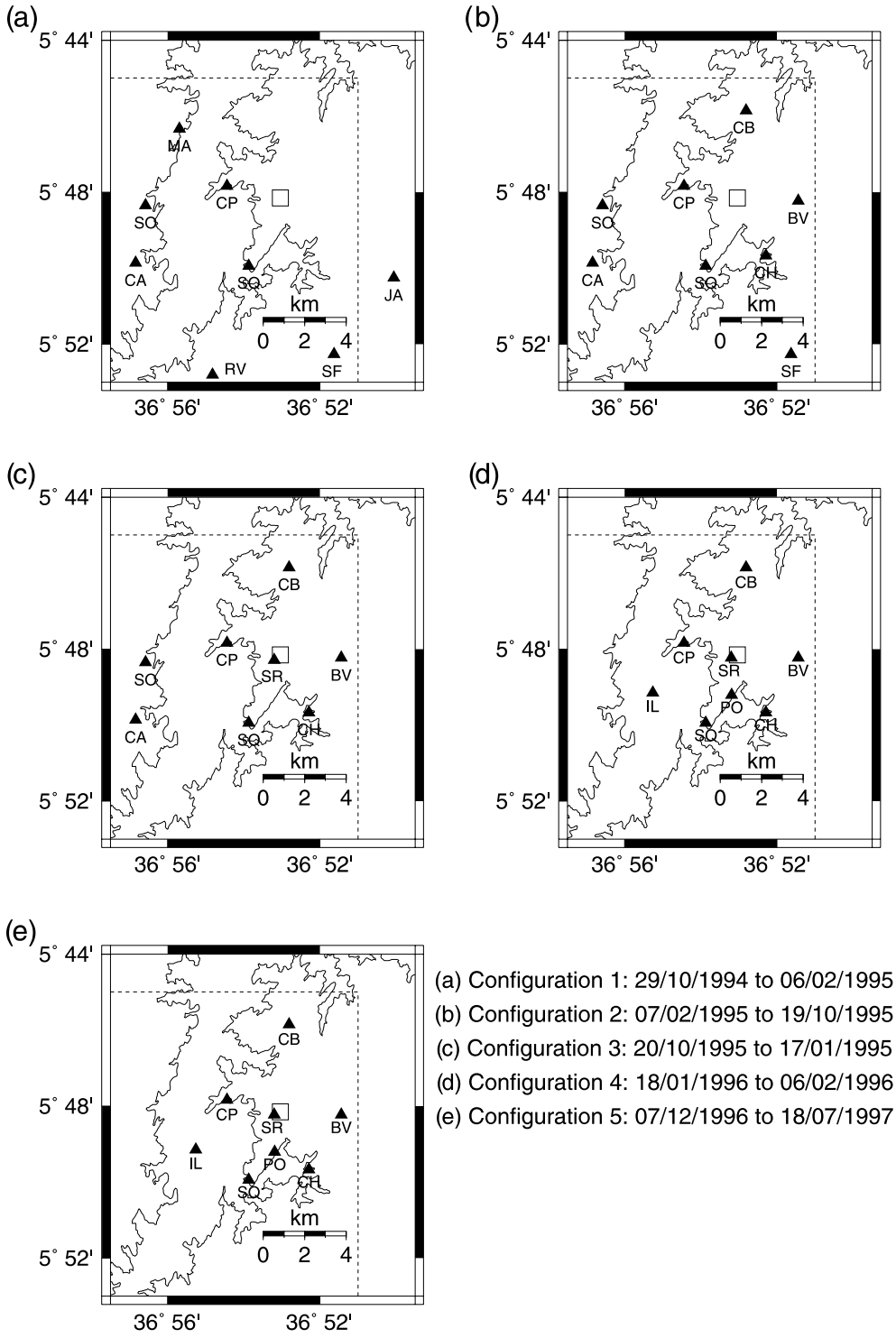

Figure 4. (a) to (e) show the five different configurations of the digital network used in this study. The dashed line on each map denotes the approximate extent of the network, i.e. the approximate detection limit for each case. The time period in which each configuration was deployed is also shown. The small open square in each figure is the location of the town of Nova São Rafael.

station should be above the event, within a cone of 45° from the vertical. The station coverage shown in Fig. 4 thus assures reliable hypocentral location of the shallowest events. The velocity model used here was the same as that used by do Nascimento (1997, 2002), which assumes an isotropic, homogeneous, infinite half-space with constant V_P and V_S values. The choice of this quite simple velocity model was made because the study region lies on Precambrian crystalline basement. Rocks of this type exhibit high rigidity and very low attenuation even in the near surface, evidenced by the simple nature of the seismograms. In order to find the V_P and V_S values, 58 events that were recorded in at least five stations with absolute timing for the *P*- and *S*-wave arrivals were used to calculate V_P/V_S

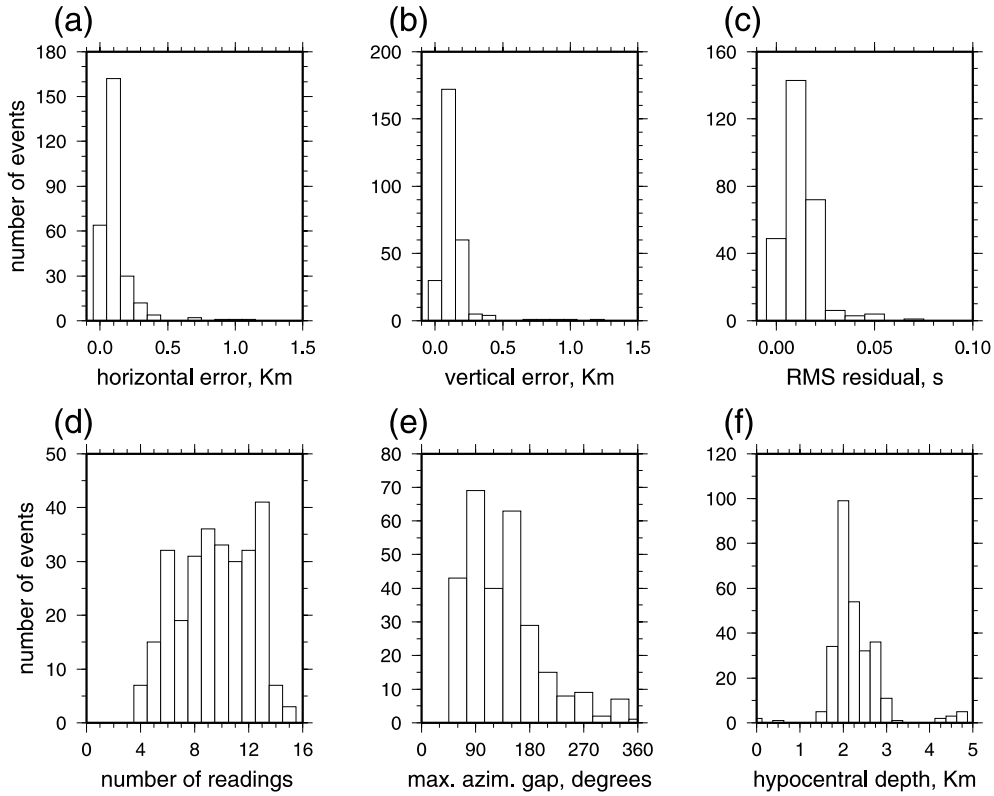

Figure 5. (a) to (f) shows hypocentre parameters obtained from analysis of the digital data using HYPO71 (Lee & Lahr 1975).

ratios via the Wadati diagram. According to the Wadati diagram for these 58 events, $V_P/V_S = 1.71$. In order to determine the V_P value, the hypocentres of the same 58 events were located using HYPO71 (Lee & Lahr 1975) with different values of V_P/V_S and V_P. The model that produced the smallest epicentral and depth estimation errors was the one that also gave $V_P/V_S = 1.71$ and $V_P = 6.00$ km s^{-1}.

Fig. 5 shows the associated HYPO71 errors and location parameters for the 286 events recorded by three or more stations of the digital network. It can be seen from Figs 5(a), (b) and (c) that most of the events have vertical and horizontal errors $\leq$0.1 km and a rms residual $\leq$0.02 s. The minimum number of readings (both *P* and *S*) is four (Fig. 5d), which indicates that the event was recorded in at least three stations. For all the hypocentral locations, besides the absolute timing of the *P* and *S* arrivals, t_P and t_S respectively, we also used traveltime differences $(t_S - t_P)$. For the spatio-temporal analysis presented in this paper, we only used those hypocentral locations with at least five readings of t_P, t_S and $(t_S - t_P)$, giving horizontal and vertical errors $\leq$0.3 and $\leq$0.4 km. This reduced our data set to 267 events but minimized the misleading artefact of the hypocentral determination algorithm whereby too few phase readings give artificially low residuals and small vertical and horizontal errors. From Fig. 5(e) we see that the maximum azimuthal gap between a located epicentre and any two stations is 180° or less for most events. Fig. 5(f) shows that the majority of events have a hypocentral depth between 1.4 and 3 km and none are deeper than 5 km. The upper cut-off to the seismicity is unlikely to be caused by poor station coverage for the reasons given above. Instead, it is most likely to be reflecting the transition to stable frictional sliding that occurs in the near surface as a result of low normal stress (see Scholz 1990, for review).

The focal mechanisms of the seismic activity from 1994 to 1997 were analysed using a programme called RAMP by Pearce (1977, 1980) and Pearce & Rogers (1989). This programme searches for double-couple point source mechanisms compatible with input *P*-wave polarities. The programme searches over a specified grid of 5° steps for the strike, dip and rake, yielding 93 312 possible solutions. In this method all the solutions fitted are considered equally compatible with the data. So, the method will not provide a single best solution, but a set of compatible solutions. In order to have a good determination of the azimuth and incident angle on the focal sphere, events (regardless of the cluster they belong to) were selected that had at least 12 readings t_S and t_P absolute and $(t_S - t_P)$ relative time readings and vertical and horizontal errors $\leq$0.1 km. The criteria used to select events for focal mechanism determination are very critical. An error in the depth determination of 0.2 km in a event 2.0 km deep can cause a 3° error in the incident angle. Moreover, an error of 0.2 km in the horizontal determination of an event distant by 2.0 km can lead to a 5° error in the azimuth determination. Fig. 6 and Table 1 shows two nodal planes found by ramp. Each solution contains a maximum of 23 polarity mismatches (the total number of polarities is 532). This small number of mismatches is an indication that all the events have a similar focal mechanism, i.e. right-lateral strike-slip motion on SW–NE oriented faults, with an E–W P-axis and N–S T-axis. The composite focal mechanism solution that we obtain here (Fig. 6) agrees with the results of Ferreira *et al.* (1995) for the previous data sets. In general, earthquake focal mechanisms in this region and in other regions in northeast Brazil are consistent

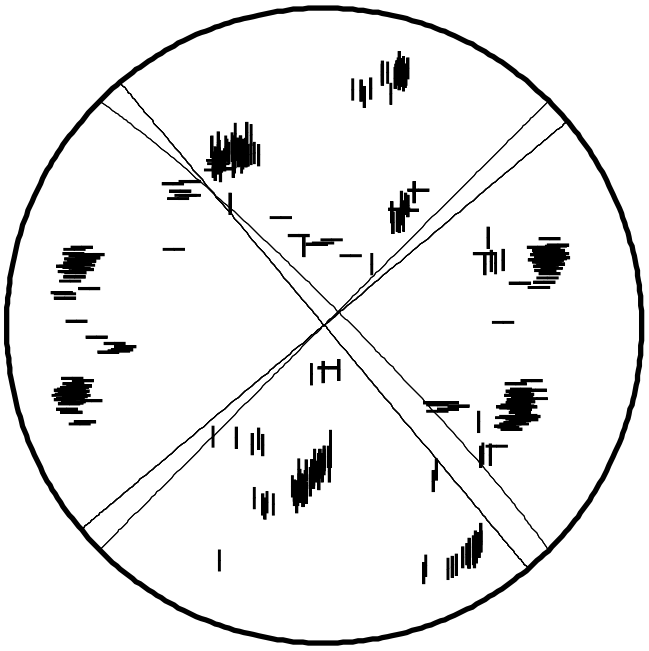

Figure 6. Composite *P*-wave first-motion polarity data for the digitally recorded events, shown on an equal area plot of the lower focal hemisphere. Compressional (positive) and dilatational (negative) first motions are indicated by vertical and horizontal bars respectively to highlight conflicting polarities more clearly. Best-fitting fault planes are also shown (see Table 1).

Table 1. Table showing the values of strike, dip and slip of the fault planes found by RAMP. Each solution contains up to 23 polarity mismatches.

Strike (°)	Dip (°)	Slip(°)
50	90	180
45	90	175

with the maximum horizontal compressive stress being oriented E–W (Assumpção 1992; Ferreira *et al.* 1998).

3 THE RELATIONSHIP BETWEEN THE WATER LEVEL AND THE SEISMICITY RECORDED BY THE DIGITAL NETWORK BETWEEN 1994 AND 1997

With such well located events provided by the digital monitoring, it is possible to examine the relationship between the migration of events and the water level variation (Figs 7 and 8). It can be noticed from Fig. 7 that the seismicity between 1994 and 1997 does not occur in a single spatial region, but is clustered in at least three different regions. We use the word cluster to denote spatially grouped events that are, in general, active over different time periods as shown below. Fig. 7 shows these three identifiable clusters. In this figure, clusters **a**, **b** and **c** are separated spatially (because the maximum location error associated with each individual earthquake is 400 m, smaller than the separation between the clusters). Note that discriminating between clusters based on focal mechanism is not possible given the consistency of focal mechanism solutions throughout the area (Fig. 6). When seen in cross-section (Fig. 7c), clusters **a** and **b** clearly occur within two elongate zones that dip steeply to the northwest. For cluster **c** the geometry is less clear but it consists of relatively few events.

For the years of digital seismic monitoring, Fig. 8(a) shows the monthly number of events recorded together with the daily water level in the reservoir. Figs 8(b), (c) and (d) show, respectively, the depth of each event, distance along a NW–SE line and distance along a SW–NE line, versus time (in years). In each of these figures different symbols are used to plot the different clusters, so that it is possible to see how the different clusters are activated in relation to the lake water level shown in Fig. 8(a). Three months in each year are labelled on the histogram to facilitate reading Fig. 8(a). The letters S, O, N and D are, respectively September, October, November and December. The spatio-temporal activity of each cluster is summarized in Tables 2 and 3.

On the 1995 May 31, a peak in water level (56.4 m), as indicated by the left hand vertical arrow in Fig. 8(a) was followed by a increase in seismicity between 1995 October 7 and 20. The time delay, therefore, was between 131 and 144 days, which is approximately 4.5 months. The seismic activity during 1995 October is the greatest in the entire 3 yr period (around 70 events in 3–4 weeks). During this month, the seismicity was also concentrated in a small portion within cluster **a**. The horizontal bar representing this month in Figs 8(b), (c) and (d) shows a depth range for the majority of these events of between 1.8 and 2.3 km and, in the SW–NE line, those events occur in a region approximately 1.5 km long and along the same fault line, within a zone $<$500 m wide, as can be observed in Fig. 8(d).

On the 1996 April 27, the water level in the Açu reservoir reached another maximum (56.7 m), as indicated by the vertical arrow on the right, in Fig. 8(a). In that year, the pronounced seismic activity started on the 1996 October 21 in cluster **b**. Therefore, the delay was 177 days, which is approximately 6.0 months. Later on 1996 November 25, cluster **c** was activated, hence a time delay of 212 days, or approximately 7 months can be inferred. These months, 1996 November and December, are also marked on Figs 8(b), (c) and (d) as horizontal bars. After 1996 November 25, clusters **b** and **c** were active at the same time but activity in a virtually ceased. Clusters **b** and **c** are are in depth ranges 2.8 to 3.0 km and 4.0 to 4.7 km, respectively.

Fig. 9 shows the time delay from the previous peak in reservoir level (in days) for each seismic event belonging to the three clusters, **a**, **b** and **c**, plotted as open symbols. The filled symbols are the data shown in column 3 of Table 3, which correspond to the peak in seismicity for each cluster as determined from analysis of individual cluster histograms. These latter values are plotted against the midpoint of the depth range shown in column 2 of Table 3. The error bars in the x-axis direction show the bin width used in the histogram analysis, 1 month. The time delay on Fig. 9 is plotted from zero (determined by the peak in water level in the reservoir) to 465 days. Obviously, the initial events seen in cluster **a** are unlikely to be a consequence of pressure diffusion from the most recent reservoir level peak because the diffusion time is too short. They may be residual seismic activity from the previous year. There is a noticeable onset of seismic activity at 100 days, so the figure has been extended to show 365 days from this onset to include all the events that are likely to be a consequence of a single reservoir level rise.

There are several observations of interest that are demonstrated by Fig. 9. First, events in each of the clusters show similar temporal behaviour: an initial onset of seismicity that rapidly reaches a peak in the frequency of seismic events for each cluster, this is then followed by a long tail throughout that the frequency of events diminishes over time. Secondly, both the onset and the peak in seismicity are delayed for increasing depth of cluster, thus demonstrating overall that the governing mechanism for event triggering is pore pressure diffusion. However, within an individual cluster there is no correlation

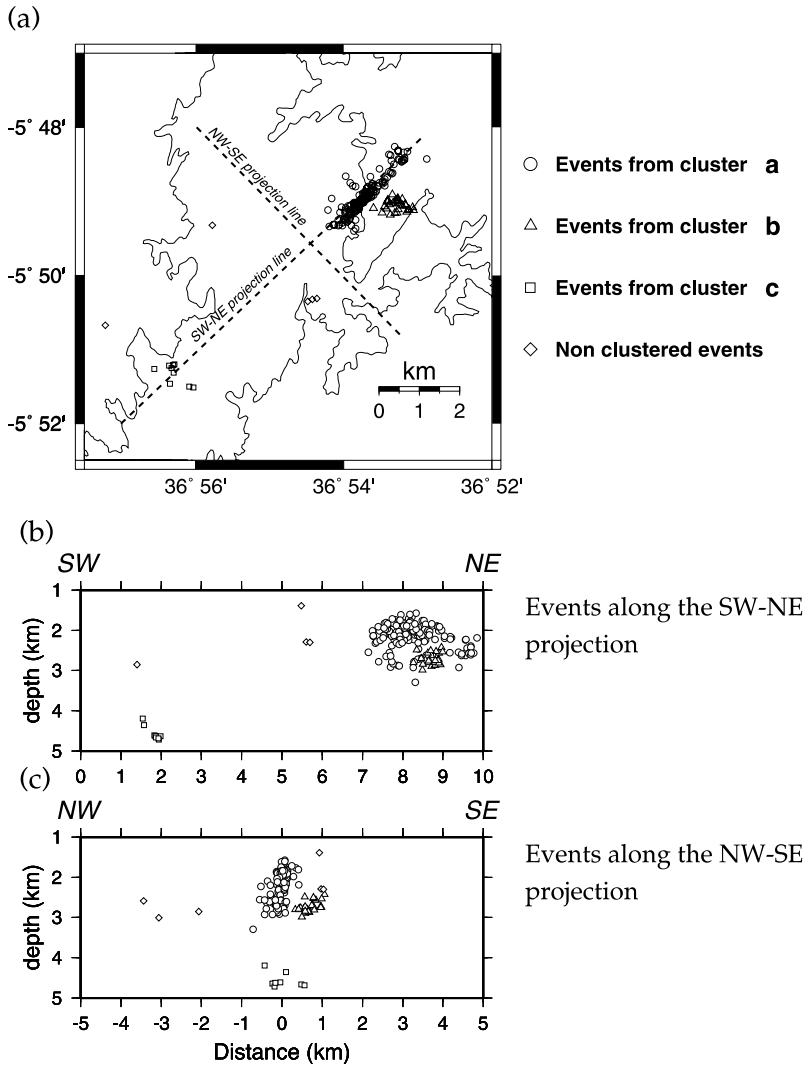

Figure 7. Shows (a) the epicentres located by the digital network in map view, (b) the projection of the hypocentres on a SW–NE line and (c) the projection of the hypocentres on a NW–SE line. The different seismicity clusters are indicated by different symbols (see Section 3 for cluster definition). The origin of the NW–SE projection line is taken to be the middle of cluster **a**.

between time delay and increasing hypocentral depth, a point that is discussed further in Section 4. The delay times shown in Table 3 indicate an average rate of diffusion of pore pressure of ≈1 km of depth per 47 days. However, cluster **a** at 2.0 km depth has a delay time of 133 days, i.e. a much longer delay than the average rate of diffusion implies. This observation suggests that the seismicity is occurring on different faults each of which has different average hydraulic properties. One simple way to approximately quantify the difference is to use the concept of seismic hydraulic diffusivity (α_s) (Talwani & Acree 1984). Talwani & Acree (1984) analysed cases of induced seismicity dominated by pore pressure diffusion and defined $\alpha_s = L^2/t$, where L is the characteristic distance between the source of pressure front and the location of the seismicity and t is the time lag between the generation of that pressure front (i.e. filling of the reservoir). They found that α_s ranges between 5×10^3 and 5×10^5 cm^2 s^{-1}. For clusters **a**, **b** and **c**, we find α_s is 3.4×10^3, 5×10^3 and 10^4 cm^2 s^{-1}, respectively. A further important feature of Fig. 9 is that the duration of seismic activity corresponding to an individual reservoir level peak reduces systematically with increasing depth. This pattern is also consistent with pore pressure diffusion as the triggering mechanism when we consider that the amplitude of the pressure wave is being attenuated over depth. As a result of this attenuation, the interval of time over which pressure exceeds a threshold value is reduced. In companion papers, we use a 3-D model of pressure diffusion to investigate both the hydraulic diffusivity and the decay in amplitude of the pressure wave for an individual fault beneath the reservoir (do Nascimento *et al.* 2004a,b).

3.1 Evidence for migration between faults: combining data from permanent station BA1 with the digital network data

In the previous section, we have shown that at least part of the explanation for an apparently poor correlation between the number of seismic events and the water level is that the depth of the triggered seismic activity varies significantly, with deeper events occurring after a longer time delay. When combined with anomalous reservoir levels during periods of drought, the lack of a clear correlation in Fig. 2 between seismicity and water level after 1989 may be largely explained. However, it is important to consider also the completeness of the seismic catalogue in case migration of the locus of the seismic

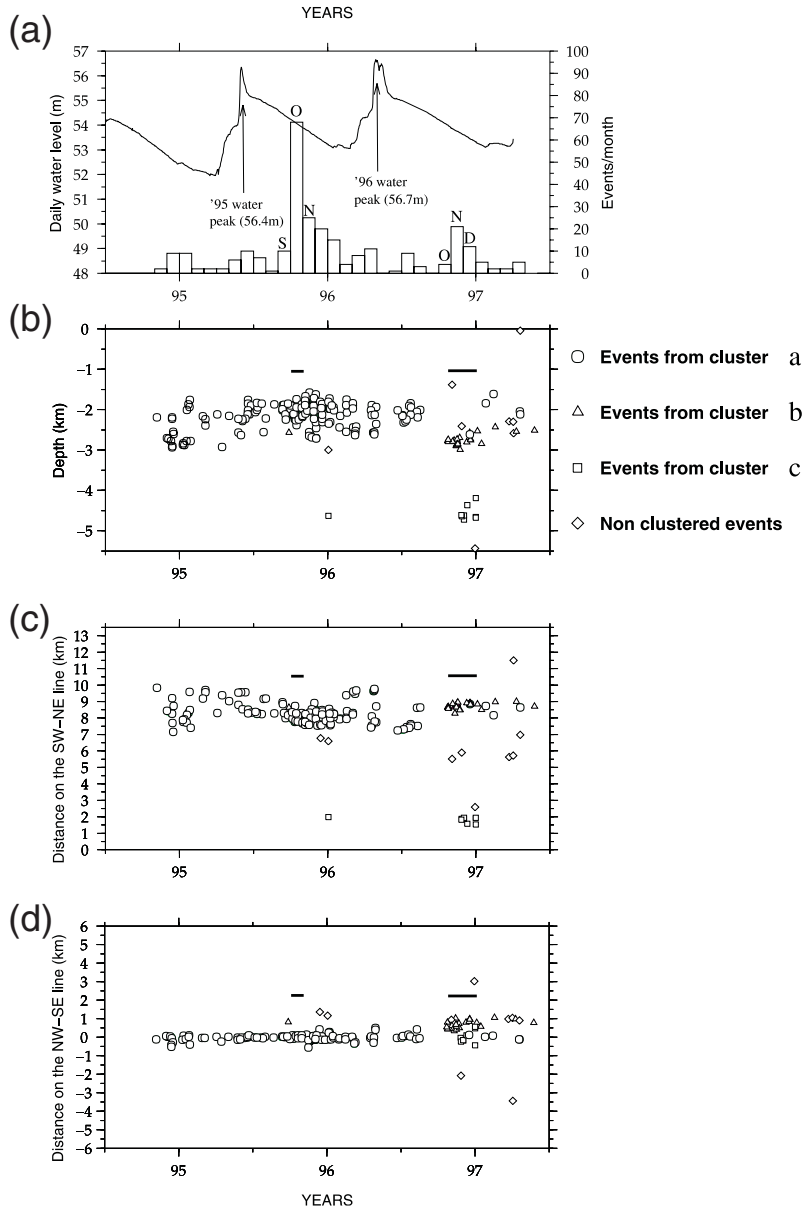

Figure 8. Spatio-temporal evolution of the seismicity from 1994 November until 1997 April. (a) Shows the daily water level variation at the Açu reservoir (top line) and the monthly histogram of events (bottom) as recorded by the digital seismic network. Arrows indicate the annual maximum water levels on 1995 May 31 and 1996 April 27, respectively. A few months of binned seismic activity are labelled to facilitate understanding: S, O, N and D are September, October, November and December, respectively. (b) Shows the temporal evolution of events with depth. A different symbol was used for each cluster as defined in Fig. 7 and Section 3. The horizontal bars highlight the months where the peak in seismic activity occurred. (c) and (d) show the temporal evolution of seismicity along SW–NE and NW–SE projection lines, as used in Fig. 7. The symbols that are used to plot the events are the same as those used in Fig. 7.

activity, and thus incomplete event detection, is another contributing factor (Ferreira *et al.* 1995).

Fig. 10(a) shows the histogram of monthly earthquake activity recorded by the permanent station BA1 and the digital seismic network. These data cover the time period of 1994 November until 1997 April. During this time period both BA1 and the digital network are known to have been operating continuously. In general terms, the histograms look very similar. The data collected by BA1 mimic the two peaks of earthquake activity in 1995 and 1996 described above. However, there are some differences in these two histograms as a result of the finite detection threshold. Events with a very small magnitude occurring near BA1 are unlikely to be detected by the digital network and small events very close to the digital network are unlikely to be detected by BA1. Over the entire period 1994 November to 1997 April (Fig. 10a) there are four time intervals when there are differences in the number of events recorded at BA1 compared to the digital network. From 1994 November until 1995 September, the number of earthquakes recorded by the digital seismic network (shaded histogram) is systematically lower than the number recorded by BA1 (white histogram). Then from 1995 October until 1996 July, the opposite is true as BA1 records systematically fewer events than the digital network. During the months of 1996 August, September and October, considerable seismicity (more than 10 events per month) was recorded by BA1 whilst very

Table 2. Activation period of events recorded by the digital seismic network and permanent station BA1 (see Section 3). With precise hypocentre determination, it is possible to observe migration of seismic events between different faults and within individual faults over different time periods. This table thus summarizes the migration pattern of the seismicity between 1994 and 1997.

Period of activation	Active seismic cluster
1994 November—1995 August 15	a, BA1 cluster
1995 August 15—1995 October 21	a
1996 October 21—1996 November 22	b
1996 November 25—1996 December 30	c, b
1997 December 30—1997 May	a, b

Table 3. Depth range and the percentage of events that occur at this depth range of each cluster shown in Fig. 7. The time delay corresponds to the time interval between the peak in water level variation and the activation of a particular cluster. Column 4 shows the per cent of all the events (for each cluster) that are in the depth range given in column 2 and that have a time delay equal (±0.5 month) to that shown in column 3.

Active seismic cluster	Depth range km	time delay (months)	per cent events
a	1.8–2.3	4.5	29
b	2.7–3.0	6.0	77
c	4.0–4.7	7.0	77

low seismicity was recorded by the digital network. Finally from 1996 November until 1997 April, the digital network again records more events than BA1.

An explanation for the differences shown in Fig. 10(a) is provided by Figs 11(a) and (b). Fig. 11(a) shows the values of the time delay between the *P*- and *S*-wave arrival times for all the events recorded at BA1, hereafter referred to as $(t_S - t_P)$ arrival times, for the period 1994 August until 1997 April. Fig. 11(b) shows the histogram of these arrival times. There are two main peaks in the distribution of $(t_S - t_P)$ arrival times at BA1, one around 0.9 s and another at 1.6 s. Although with one single-component station one cannot determine a hypocentre, it is possible to calculate the distance of those events from the station. If a homogeneous half-space is used, where values of $V_P/V_S = 1.71$ and $V_P = 6.00$ km s^{-1} are valid for the entire region, it is possible to write that $\Lambda = 8.45(t_S - t_P)$, Λ being the distance from the station to the event in km. Using the values of $(t_S - t_P)$ of the two main peaks (at 0.9 and 1.6 s), it is found that such events are occurring mainly at two discrete hypocentral distances of ≈7.6 and ≈13.5 km respectively from BA1. Taking the depth range of the seismicity to be between 1 and 5 km (Fig. 8b), these distances convert to epicentral distances of 5.7–7.5 and 12.6–13.5 km respectively from BA1. The main area of seismic activity recorded by the digital network to the south of Nova São Rafael is approximately 12–14 km SSW of BA1, which most likely corresponds to the peak at 1.6 s seen in Fig. 11(b). Thus, it is the peak at 0.9 s that is of interest here as it suggests the presence of another seismicity cluster closer to BA1 that was not recorded by the digital network. The dashed box in Fig. 10(b) shows the approximate detection limit of the digital network. The detection limit of the digital network does not extend more than 5 km north of the town of Nova São Rafael. Therefore, the digital network was very unlikely to detect the seismicity cluster close to BA1. In Table 2 we therefore refer to this as the BA1 cluster. In Fig. 10(b) the smaller dashed circle (radius 5.7 km) is used to indicate the epicentral distance of events with $(t_S - t_P) = 0.9$ s, assuming a hypocentral depth =5.0 km. The larger circle (radius 7.5 km) is to mark epicentral distances when the hypocentral depth equals 1.0 km.

It can be concluded from this simple analysis that from 1994 August until 1995 December, as indicated by arrows on Fig. 11(a), two areas were seismically active: one near Nova São Rafael (i.e. cluster **a** of this study) and another one 5.7–7.5 km from BA1. Because only the $(t_S - t_P)$ arrival times are available, it is not possible to constrain the actual location of these events. However, in 1989, Ferreira *et al.* (1995) did locate a few events 5–6 km SSE of BA1 shown in Fig. 3. Therefore, it is possible that the cluster of activity at an epicentral distance of 5.7–7.5 km from BA1 occurred in the same location. The fact that, for the period 1994 November to 1995 September, the number of events recorded per month (typically <10) by the digital network is much smaller than the number recorded by BA1 per month (typically 10–30 per month) (Fig. 10a), suggests that this additional cluster of activity near BA1 was relatively significant. In particular, there is a peak in activity recorded by BA1 in 1995 January that is approximately 6 months after the peak water level (54.3 m) in July 1994. This peak is comparable in size to the peak that occurred in 1996 November–December when clusters **b** and **c** were active south of Nova São Rafael.

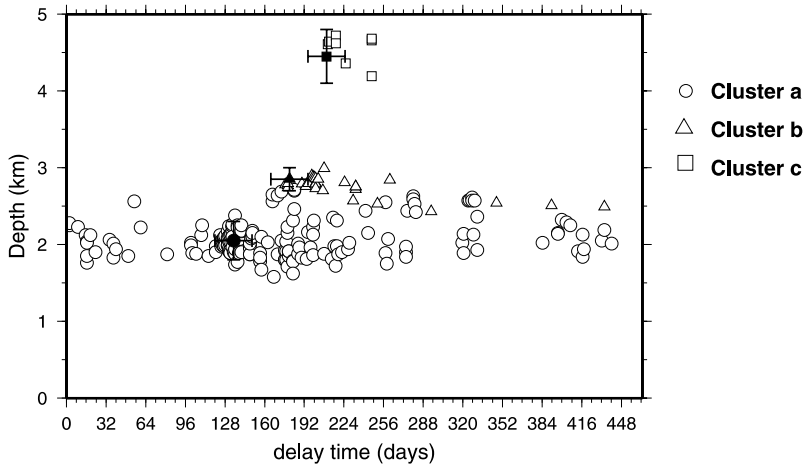

Figure 9. Time delay (in days) for each earthquake, with open symbols denoting the cluster (**a**, **b** or **c**, as shown in Figs 7 and 8). The filled symbols with error bars are the data shown in Table 3. For the latter, the mid-point of the depth range shown in Table 3 is plotted and the vertical error bar indicates the depth range (see column 2 of Table 3). The time delay is from column 3 of Table 3, ±0.5 month in each case.

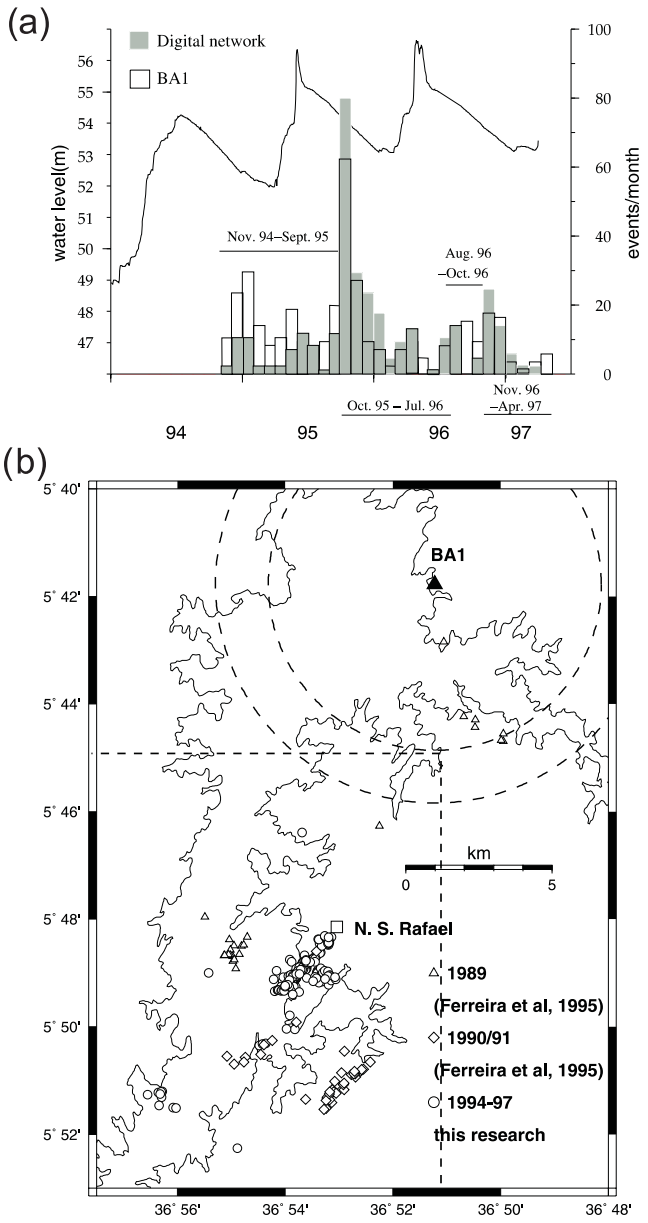

Figure 10. (a) Shows monthly earthquake activity versus water level for the period 1994–1997. The shaded bars represent the histogram of the number of events detected by the digital seismic network. The white bars are the histogram of the number of events detected by the permanent station BA1 located in Fig. 3. The continuous line shows the variation in water level of the reservoir. The horizontal bars indicate time periods discussed in Section 3.1. (b) Map showing the same seismicity data as Fig. 3 and the location of permanent station BA1. The smaller dashed circle around station BA1 marks the epicentral locations of events with $(t_S - t_P)$ arrival times of 0.9 s, assuming a hypocentral depth of 5.0 km (see Fig. 11). The larger dashed circle marks epicentres with $(t_S - t_P)$ arrival times of 0.9 s, but assuming a hypocentral depth of 1.0 km. The dashed square denotes the approximate detection limit of the digital network as shown in Fig. 3.

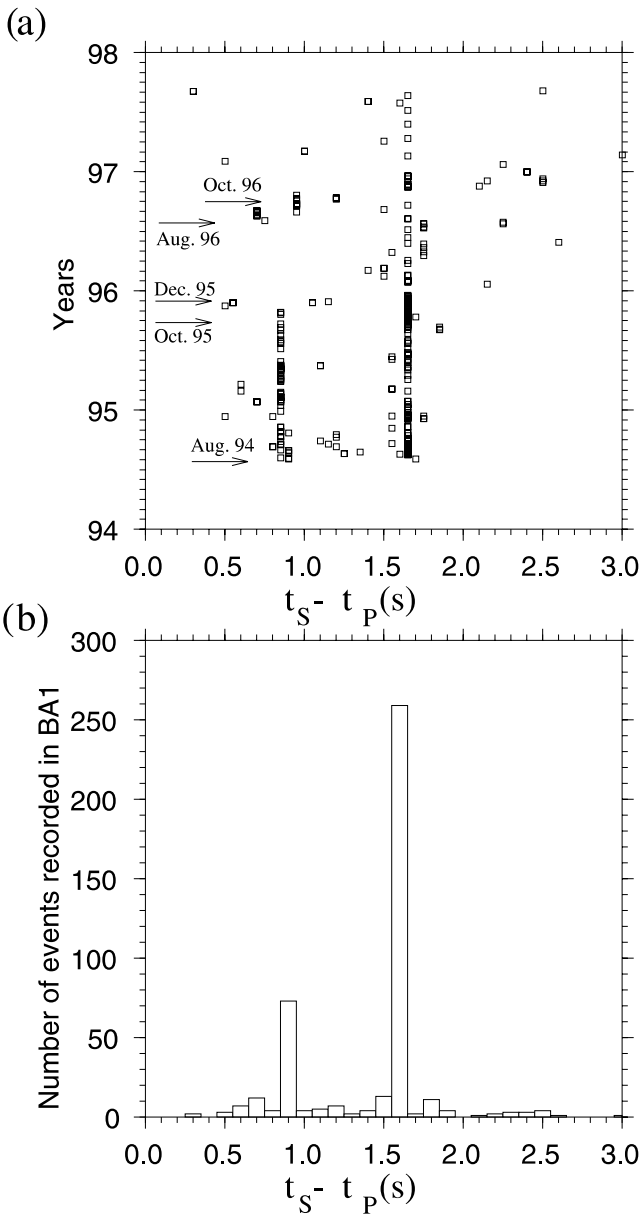

Figure 11. Distribution of $(t_S - t_P)$ arrival times as recorded by BA1. (a) Shows the values of $(t_S - t_P)$ arrival times versus time. Arrows indicate the beginning of a month/year in which the seismicity was in more than one seismic area of the reservoir, or it migrated. (b) Shows the histogram of the distribution of $(t_S - t_P)$ arrival times of events recorded by BA1. The peak at 0.9 s relates to a cluster of activity ≈5–6 km away from BA1 and is referred to as BA1 cluster in Table 2 (see Section 3.1 for explanation).

There is further evidence for spatial migration in Fig. 10(a). Overall, from 1995 October until 1996 August, the areas southwest of Nova São Rafael were mainly active (clusters **a**, **b** and **c**), although some minor activity persisted near BA1 between 1995 October and 1995 December (Fig. 11a). Consequently more seismicity was recorded by the digital network than by BA1 in this time interval (1995 October to 1996 August). However, from 1996 August until the end of 1996 October there was, once more, significant seismicity occurring near BA1 as well as continued activity to the south of Nova São Rafael. This explains why the white histogram bars (BA1) in Fig. 10 are again higher than the shaded bars (digital network) for this time period. Then from 1996 November onwards, Fig. 11(a) shows that the previously active area 5.7–7.5 km from BA1 is quiescent.

There is ample evidence, therefore, of a repeated shift of the locus of seismic activity over several kilometers during the time period when the digital network was operating. Although the time delays between peak water level and peak seismic activity for 1995 and

1996 remain unchanged (see Section 3 and Table 2), migration of seismic activity from zone to zone clearly contributes to the complex behaviour shown in Fig. 2. Note that there is no systematic pattern to the migration. In some cases the activity shifts in a direction parallel to the long axis of the reservoir. In other instances the shift is to greater distances from the reservoir edge, but there is no consistent direction to the lateral migration as is clear from Fig. 3.

4 DISCUSSION AND CONCLUSIONS

RIS in the Açu area between 1987 and 1997 occurs in well-defined clusters aligned in NE trending elongate zones. These zones are subparallel to the strike of fault planes inferred from the earthquake focal mechanisms (Fig. 3). Thus, we interpret these clusters to be the manifestation of faults that most likely correspond to weakly developed brittle faults mapped in this area. The seismicity is observed to migrate between these faults and within individual faults over different periods of time. There is no systematic trend to the lateral migration relative to the edge of the reservoir. The results of the spatio-temporal analysis are summarized in two tables. Table 2 summarizes the spatio-temporal evolution of events located by the digital network and the permanent station BA1. In 1994 November–December, we infer that most of the seismic activity was clustered in an area approximately 6 km to the south of BA1 although the location of these events is not well constrained. This area remained intermittently active over the remainder of the time period during which the digital network was operating, but the locus of activity shifted to the south of Nova São Rafael, well within the area covered by the digital network. For the events that were detected by the digital network it was possible to obtain good constraints on hypocentral locations as well as times of activation. Consequently, for these events it is possible to relate the activation of each cluster to the delayed effect of an increase in water level in the reservoir. Table 3 shows the values of the delays and the depths at which the seismic clusters located by the digital network were activated. We found that the time delay between the maximum in water level and the subsequent activation of clusters of seismic events increased as the average hypocentral depth of the clusters increased. More detailed analysis in Fig. 9 also showed that the duration of seismicity within each cluster corresponding to an individual reservoir level peak reduced systematically for clusters at greater depth. These results are consistent with the diffusion of fluid pressure as the dominant mechanism for triggering events at the Açu reservoir. The small size of Açu reservoir (only 2.4×10^9 m^3) suggests that the change in stress as a result of the load of the reservoir itself is negligible.

There are several features of the data that probably indicate the nature of the rock mass through which the fluid is diffusing. First, the elongate appearance of the earthquake clusters, particularly in map view (Fig. 3), implies that there are a number of discrete faults embedded within the rock volume. The fluid is moving preferentially through these faults. Secondly, the relationship between average time delay and average hypocentral depth obtained for the digitally recorded seismicity (Fig. 9) indicates that the individual clusters occur on faults that have different average hydraulic properties. In particular, clusters **a** and **b** occur on faults that have slightly lower average conductivities compared to the fault on which cluster **c** is located. Thirdly, within each cluster the events are spatially and temporally scattered (Fig. 9). This latter feature of the data may be attributed to a heterogeneous permeability structure within each fault. Variations in permeability lead to localized pathways of faster flow adjacent to areas of slow flow and hence the time at which the triggering pore pressure is reached at a given depth will vary. Finally, the clusters are of limited spatial extent. This may be simply reflecting the fact that the faults are of finite dimensions, or it may be indicating that the events are occurring in the patches of the fault plane where the failure threshold is lower than adjacent areas.

Numerical models so far developed to investigate RIS are either 2-D homogeneous models (Roeloffs 1988; Talwani 1997), or 2-D homogeneous models containing a 1-D homogeneous fault (Bell & Nur 1978; Simpson & Narasimhan 1992). The spatio-temporal pattern of seismicity analysed here shows a clear example of RIS exhibiting complex 3-D migratory behaviour. The only 3-D models for RIS, by Kalpna (2000) and Chen & Talwani (2001), assume a homogeneous medium, which is clearly inconsistent with the observations described above. The only model that does explicitly consider heterogeneity is a 2-D model that includes a heterogeneous matrix but a homogeneous fault (Lee & Wolf 1998). In two related papers (do Nascimento *et al.* 2004a,b), we present a model that incorporates 3-D geometry and realistic boundary conditions to investigate the pressure diffusion in the area and the role of structural heterogeneity (i.e. faults with heterogeneous properties) in order to provide new insights on the mechanisms that may cause the migratory behaviour observed at Açu.

ACKNOWLEDGMENTS

AFdN was supported by a scholarship from the Conselho Nacional de Desenvolvimento Científico e Tecnológico (CNPq, Brazil). AFdN thanks the projects Caracterização geomecânica de reservatórios heterogêneos and Falhas e fraturas naturais: aplicações na caracterização de reservatórios from FINEP/CTPETRO and the Agência Nacional do Petróleo—ANP, Brazil for financial support. The authors thank Eduardo de Menezes and Drs M.K. Takeya and J.M. Ferreira (Laboratório Sismológico da UFRN, Brazil) for their efforts in the field campaigns. The authors also thank Dr F.H.R. Bezerra for helpful comments. GMT Wessel & Smith (1998) was used to display most of our results. The authors are grateful to Nano Seeber, an anonymous reviewer and the editor, Raul Madariaga, for constructive comments on this manuscript.

REFERENCES

Amaral, C.A., 1997. Correlação entre contexto morforestrutural e sismicidade nas regiões de João Câmara e São Rafael (RN), unpublished, *MSc Thesis* UFRN, Natal, in Portuguese.

Assumpção, M., 1992. The regional intraplate stress field in south america, *J. geophys. Res.,* **97**(B8), 11 889–11 903.

Beck, J.L., 1976. Weight-induced stresses and recent seismicity at lake Oroville and California, *Bull. seism. Soc. Am.,* **66**(4), 1121–1131.

Bell, M.L. & Nur, A., 1978. Strength changes due to reservoir-induced pore pressure and stresses and applications to lake Oroville, *J. geophys. Res.,* **83**(B9), 4469–4482.

Chen, L. & Talwani, P., 2001. Mechanism of initial seismicity folowing impoundment of the Monticello Reservoir, South Carolina, *Bull. seism. Soc. Am.,* **91**(6), 1582–1594.

CPRM, 1982. Projeto Scheelita do Seridó, Mapa Geológico Integrado, 1:250,000 CPRM Brazil.

do Nascimento, A.F., 1997. Estudo da sismicidade induzida pelo reservatório da barragem do Assu (RN), unpublished, *MSc Thesis* UFRN, Natal, in Portuguese.

do Nascimento, A.F., 2002. The role of pore pressure diffusion in a reservoir-induced seismicity site in NE Brazil, unpublished, *PhD thesis* University of Edinburgh, UK.

do Nascimento, A.F., Lunn, R.J. & Cowie, P.A., 2004a. Modelling the heterogeneous hydraulic properties of faults using constraints from Reservoir Induced Seismicity, *Geophys. J. Int.,* accepted for publication.

do Nascimento, A.F., Lunn, R.J. & Cowie, P.A., 2004b. Numerical modelling of pore pressure diffusion in a reservoir-induced seismicity site in ne brazil, *Geophys. J. Int.,* accepted for publication.

Ferreira, J.M., Oliveira, R.T., Assumpção, M., Moreira, J. A.M., Pearce, R.G. & Takeya, M.K., 1995. Correlation of seismicity and water level—an example from Northeastern Brazil, *Bull. seism. Soc. Am.,* **85,** 1483–1489.

Ferreira, J.M., Oliveira, R., Takeya, M.K. & Assumpção, M., 1998. Superposition of local and regional stresses in northeast Brazil: evidence from focal mechanism around the Potiguar marginal basin, *Geophys. J. Int.,* **134,** 341–355.

Gough, D.I., 1969. Incremental stress under a two-dimensional artificial lake, *Can. J. Earth Sci.,* **6,** 1067–1075.

Gough, D.I. & Gough, W.I., 1970. Load-induced earthquakes at Lake Kariba—ii, *Geophys. J. R. astr. Soc.,* **21,** 79–101.

Gupta, H.K., 1992. *Reservoir-induced earthquakes,* **Vol. 64,** Elsevier, New York.

Jardim de Sá, E.F., 1994. A Faixa Seridó (Província Borborema, NE do Brasil) e o seu significado Geodinâmico na Cadeia Brasiliana/Pan-Africana, unpublished, *PhD thesis*, Universidade de Brasília, Brasilia, in Portuguese.

Kalpna, R.C., 2000. Green's function based stress diffusion solutions in the porous elastic half space for time varying finite reservoir loads, *Phys. Earth planet. Int.,* **120,** 93–101.

Lee, M.-K. & Wolf, L.W., 1998. Analysis of fluid pressure propagation in heteregeneous rocks: Implications for hydrologically-induced earthquakes, *Geophys. Res. Lett.,* **25**(13), 2329–2332.

Lee, W.H.K. & Lahr, J.C., 1975. HYPO71 (revised): a computer program for determining hypocenter, magnitude, and first motion pattern of local earthquakes, *US Geological Survey, Open File Rep.,* 75–311.

Pearce, R.G., 1977. Fault plane solutions using relative amplitude methods of P and pP, *Geophys. J. Roy. astr. Soc.,* **50,** 381–394.

Pearce, R.G., 1980. Fault plane solutions using relative amplitudes of P and pP: further studies., *Geophys. J. R. astr. Soc.,* **60,** 469–487.

Pearce, R.G. & Rogers, R.M., 1989. Determination of eartquake moment tensors from teleseismic relative amplitude observations, *J. geophys. Res.,* **94,** 775–786.

Petrobras, 1986. Mapa Geológico da Bacia Potiguar, Anexo 14, Folha Açu, scale 1:1,000,000. Unpublished map.

Roeloffs, E.A., 1988. Fault stability changes induced beneath a reservoir with cyclic variations in water level, *J. geophys. Res.,* **93**(B3), 2107–2124.

Scholz, C.H., 1990. *The mechanics of earthquakes and faulting,* 2nd edn, Cambridge University Press, Cambridge.

Simpson, D.W. & Narasimhan, T.N., 1992. Inhomogeneities in rock properties and their influence on reservoir induced seismicity, in, *Induced seismicity,* pp. 345–359, ed. Knoll, P., Balkema, Rotterdam.

Talwani, P., 1976. Earthquakes associated with the Clark Hill Reservoir, South Carolina—a case of induced seismicty, *Eng. Geol.,* **10,** 239–253.

Talwani, P., 1997. On the nature of reservoir-induced seismicity, *Pageoph,* **150,** 473–492.

Talwani, P. & Acree, S., 1984. Pore pressure diffusion and the mechanism of reservoir-induced seismicity, *Pageoph,* **122,** 947–965.

Wessel, P. & Smith, W.H.F., 1998. New, improved version of Generic Mapping Tools released, *EOS, Trans. Am. geophys. Un.,* **79**(**47**), 579.

Zoback, M.D. & Hickman, S., 1982. In situ study of the physical mechanisms controlling induced seismicity at monticello reservoir and south carolina, *J. geophys. Res.,* **87**(**B8**), 6959–6974.